



Pd Clusters on Schiff Base–Imidazole-Functionalized MOFs for Highly Efficient Catalytic Suzuki Coupling Reactions

Yangqing Liu^{1†}, Jingwen Sun^{1†}, Lan Fan² and Qi Xu^{1*}

¹School of Chemistry and Chemical Engineering, Key Laboratory Under Construction for Volatile Organic Compounds Controlling of Jiangsu Province, Yancheng Institute of Technology, Yancheng, China, ²Yancheng Lanfeng Environmental Engineering Technology Co., LTD, Yancheng, China

OPEN ACCESS

Edited by:

Xiao-Yu Yang,
Wuhan University of Technology,
China

Reviewed by:

Hexing Li,
Shanghai Normal University, China
Benjaram M. Reddy,
Indian Institute of Chemical
Technology (CSIR), India

*Correspondence:

Qi Xu
yxcqsteve@163.com

[†]These authors have contributed
equally to this work

Specialty section:

This article was submitted to
Catalysis and Photocatalysis,
a section of the journal
Frontiers in Chemistry

Received: 29 December 2021

Accepted: 20 January 2022

Published: 01 March 2022

Citation:

Liu Y, Sun J, Fan L and Xu Q (2022) Pd
Clusters on Schiff Base–Imidazole-
Functionalized MOFs for Highly
Efficient Catalytic Suzuki
Coupling Reactions.
Front. Chem. 10:845274.
doi: 10.3389/fchem.2022.845274

Subnanometer noble metal clusters have attracted much attention because of abundant low-coordinated metal atoms that perform excellent catalytic activity in various catalytic processes. However, the surface free energy of metals increases significantly with decreasing size of the metal clusters, which accelerates the aggregation of small clusters. In this work, new Schiff base–imidazole-functionalized MOFs were successfully synthesized *via* the postsynthetic modification method. Highly dispersed Pd clusters with an average size of 1.5 nm were constructed on this functional MOFs and behaved excellent catalytic activity in the Suzuki coupling of phenylboronic acid and bromobenzene (yield of biaryl >99%) under mild reaction conditions. Moreover, the catalyst can be reused six times without loss of activity. Such catalytic behavior is found to closely related to the surface functional groups that promote the formation of small Pd⁰ clusters in the metallic state.

Keywords: Pd clusters, subnanometer size, Schiff base, Suzuki coupling reaction, metal organic frameworks

INTRODUCTION

Subnanometer noble metal clusters (SNMCs) with dimensions in the range from a few to dozens of angstroms have drawn focused attention (Diez and Ras, 2011; Imaoka et al., 2017; Wang et al., 2020; Yamamoto et al., 2020; Dong et al., 2021). With most of the constitutional atoms exposed to the surface, which is an unsaturated coordination environment and have higher reactivity than those in the bulk, SNMCs perform excellent catalytic activity and selectivity when serving as catalysts, thus, dramatically increasing the utilization efficiency of noble metals. The catalytic activity of SNMCs will be further improved as the size decreases, due to the surface atomic structure, electronic structure, and defects will change significantly. However, because of high surface energy, a too tiny size could lead to aggregation and particle growth (Tang et al., 2017; Si et al., 2018; Xin et al., 2018). A solution to the critical issue is to apply a nanoporous supporting material, such as graphene (Gu et al., 2017; Liu et al., 2019), carbon nanofibers (Eid et al., 2019), C₃N₄ (Yang et al., 2021; Zhang et al., 2021), and porous SiO₂ (Peng et al., 2019). Nevertheless, some disadvantages, such as leaching and aggregation of SNMCs, exist during the catalytic process by using these materials as support, which, thus, weaken the catalytic activity (Gu et al., 2017; Liu et al., 2019; Zhang et al., 2021). Therefore, it is of great importance to design supporting materials that cannot only make ultrafine SNMCs with uniformity and high dispersion but also endow the obtained catalysts with excellent catalytic activity.

Metal–organic frameworks (MOFs) are a fascinating family of porous crystalline materials assembled with inorganic metal nodes and organic linkers, possessing large internal surface areas, well-defined structures, and tunable chemical properties (Lee et al., 2009; Li et al., 2012; Furukawa et al., 2013). These features confer their popular applications in heterogeneous catalysis, particularly when they are used as support for noble metal (e.g., Pd, Au, Ru, and Pt) nanoparticles (MNPs) (He et al., 2018; Han et al., 2019; Chen et al., 2021; Khan et al., 2021). On the one hand, the permanent porosity and uniform channels of MOFs make them particularly suitable for the efficient immobilization of MNPs that protect the MNPs from sintering and aggregation without inhibiting the diffusion of the reactants and products. On the other hand, the organic linkers or the metal nodes of MOFs can also be used as unique functional moieties, and the interaction between MOFs and MNPs can trigger excellent synergistic effects, affording properties that are superior to the individual components (Fang et al., 2018; He et al., 2018; Mouarrawis et al., 2018; Han et al., 2019; Khan et al., 2021). Su et al. constructed a series of novel MOFs based on redox-active tetrathiafulvalene (TTF) organic linkers. Ultra-small noble metal (Ag, Pd, and Au) nanoparticles were successfully generated *in situ* and stabilized in the MOF cavity due to the reductive TTF moieties (Su et al., 2020). Recently, Guo and coworkers synthesized highly dispersed ultrafine platinum (Pt) particles with a size of <1.5 nm anchored onto amino group-functionalized MOFs (NH₂-Ce-MOFs). It was found that the presence of -NH₂ groups in NH₂-Ce-MOFs played a crucial role in anchoring Pt species with high dispersion on the MOF framework (Guo et al., 2021). Based on these reports, the development of SNMC/MOF materials for noble metal catalysis will exert a significant impact on conventional chemical industrial processes.

In this work, we constructed a novel Schiff base–imidazole-functionalized MOFs and apply the MOFs as support to anchor Pd⁰. Pd⁰ clusters were uniformly dispersed in the MOFs with an average size of 1.5 nm, which is a very small size by using MOFs as support, as we know. The sub-1.5 nm Pd⁰ cluster-supported MOFs performed excellent activity in the Suzuki coupling reactions and behaved with high stability.

EXPERIMENTAL METHODS

Chemicals

All chemicals and reagents were obtained from commercial sources and used as received. Specifically, zirconium chloride (ZrCl₄), anhydrous N,N-dimethylformamide (DMF), 2-aminoterephthalic acid (H₂BDC-NH₂), 4-imidazolecarboxaldehyde (Im-CHO), and palladium acetate (Pd(OAc)₂) were purchased from Aladdin.

Catalyst Preparation

Synthesis of UIO-66-NH₂

UIO-66-NH₂ was prepared following a procedure previously reported (Zhang et al., 2016) with slight modifications. In a typical synthetic process, ZrCl₄ (0.24 g, 1.029 mmol) was

dissolved in DMF (60 ml) by sonication for 5 min. Then the ligand H₂BDC-NH₂ (0.186 g, 1.029 mmol) and deionized water (0.15 ml) successively dropped into the mixture, and stirring was initiated until all precursors were completely dissolved. The obtained mixture was transferred into a 100-ml Teflon-lined stainless-steel autoclave, and kept at 393 K for 24 h under static conditions. After cooled to room temperature (r.t.), the obtained yellow precipitate was separated by centrifugation at 10,000 rpm for 5 min and thoroughly washed with DMF and methanol three times, respectively. Finally, the yellow powder was freeze dried in a freeze dryer prior to experiments.

Synthesis of UIO-66-SB-Im

The Schiff base–imidazole-functionalized MOFs was prepared by a postmodification strategy. Typically, UIO-66-NH₂ (0.175 g, 0.1 mmol) was dispersed in 30 ml of ethanol by sonication for 5 min. Then Im-CHO (0.144 g, 1.5 mmol) was added into the mixture, and the resulting mixture was refluxed at 80°C for 24 h. The formed yellow solid was filtered and washed with abundant ethanol three times and then freeze dried in a freeze dryer.

Synthesis of Pd⁰@UIO-66-SB-Im

The acetone solution of Pd(OAc)₂ was first prepared by dissolving Pd(OAc)₂ (0.02 g) in 5 ml of acetone. Then UIO-66-SB-Im (0.2 g) was added into the above solution, and the mixture was subsequently stirred at room temperature (r.t.) for 24 h. Afterward, the precipitate was collected by centrifugation and washed with abundant acetone three times. The as-synthesized sample was freeze dried in a freeze dryer and denoted as Pd²⁺@UIO-66-SB-Im. The Pd²⁺ in the as-synthesized sample Pd²⁺@UIO-66-SB-Im was subsequently reduced to Pd⁰ in a stream of 5% H₂/N₂ (75 cm³/min), with the temperature ramped from 20°C to 200°C (at 3°C/min) and held at 200°C for 2 h to obtain Pd⁰@UIO-66-SB-Im. For contrast, Pd⁰@UIO-66-NH₂ was prepared through a similar process by changing the support to UIO-66-NH₂.

Catalyst Characterization

Pd contents were estimated on an OPTMA 20,000-V inductive coupled plasma mass spectroscopy (ICP). Elemental analyses were performed on a CHN elemental analyzer Vario EL cube. Power X-ray diffraction (PXRD) patterns were recorded on a Panalytical X'Pert³ Powder diffractometer with Cu K α radiation ($\lambda = 1.5406 \text{ \AA}$) from $2\theta = 5^\circ - 80^\circ$, at a scan rate of 0.2° s^{-1} , with the beam voltage and current of 45 kV and 200 mA, respectively. Scanning electron microscopy (SEM) images were recorded on an FEI Nova Nano SEM 450 Prime scanning electron microscope. Transmission electron microscopy (TEM) images were obtained from a JOEL JEM-1400plus transmission electron microscope at an accelerating voltage of 200 kV. Fourier transform infrared spectroscopy (FTIR) spectra in the wavenumber range of $4,000 - 800 \text{ cm}^{-1}$ were recorded on an Agilent Cary 660 FTIR Spectrometer. The nitrogen (N₂) sorption isotherms were measured at the temperature of liquid nitrogen (77 K) by using a BELSORP-MINI analyzer with the samples being

degassed at 100°C for 3 h before analysis. The surface area and pore-size distribution curves were calculated by the Brunauer–Emmett–Teller (BET) and density functional theory (DFT) method, respectively. X-ray photoelectron spectroscopy (XPS) measurement was performed on ESCALAB 250Xi with a monochromatic Mg-K α source operated at 20 kV. All binding energies were calibrated by using the contaminant carbon (C1s = 284.8 eV) as the reference.

Catalyst Preparation

The Pd-catalyzed Suzuki coupling reactions of phenylboronic acid and bromobenzene were carried out in a 25-ml Schlenk tube. Generally, phenylboronic acid (3 mmol), bromobenzene (2 mmol), NaHCO₃ (4 mmol), Pd⁰@UIO-66-SB-Im (0.103 mol % Pd based on bromobenzene), dimethylacetamide (DMA, 5 ml), and 550 μ l of diethyleneoxide (internal standard) were successively added into a 25-ml Schlenk tube. The tube was closed and placed in a preheated oil bath. The reaction was conducted under stirring at 90°C for 7 h. After the reaction, the tube was cooled on ice to quench the reaction, and Pd⁰@UIO-66-SB-Im was separated from the reaction medium by centrifugation and the products were analyzed by gas chromatograph [GC: Agilent GC6890N with a flame ionization detector (FID) and an HP-5 column (30 m, 0.25 mm inner diameter)]. The yield was determined with a calibration curve method.

For investigating the heterogeneous nature of the catalyst Pd⁰@UIO-66-SB-Im, a hot filtration test was applied. A mixture of phenylboronic acid (3 mmol), bromobenzene (2 mmol), NaHCO₃ (4 mmol), dimethylacetamide (DMA, 5 ml) and the catalyst Pd⁰@UIO-66-SB-Im (0.103 mol% Pd based on bromobenzene) was stirred at 90°C. After 1.5 h, the catalyst was separated by centrifugation, the reaction solution was still stirred for 4.5 h, and the products were detected by GC at the reaction times of 0.5, 1.5, 2.5, 3.5, and 4.5 h.

In order to test the durability of the Pd⁰@UIO-66-SB-Im in the Suzuki coupling reaction system, the Pd⁰@UIO-66-SB-Im was recovered from the reaction mixture by centrifugation after the completion of previous catalytic reaction cycle, and washed with deionized water and ethanol, freeze dried in a freeze dryer, and then directly charged to the next run.

RESULTS AND DISCUSSION

Structure Analysis

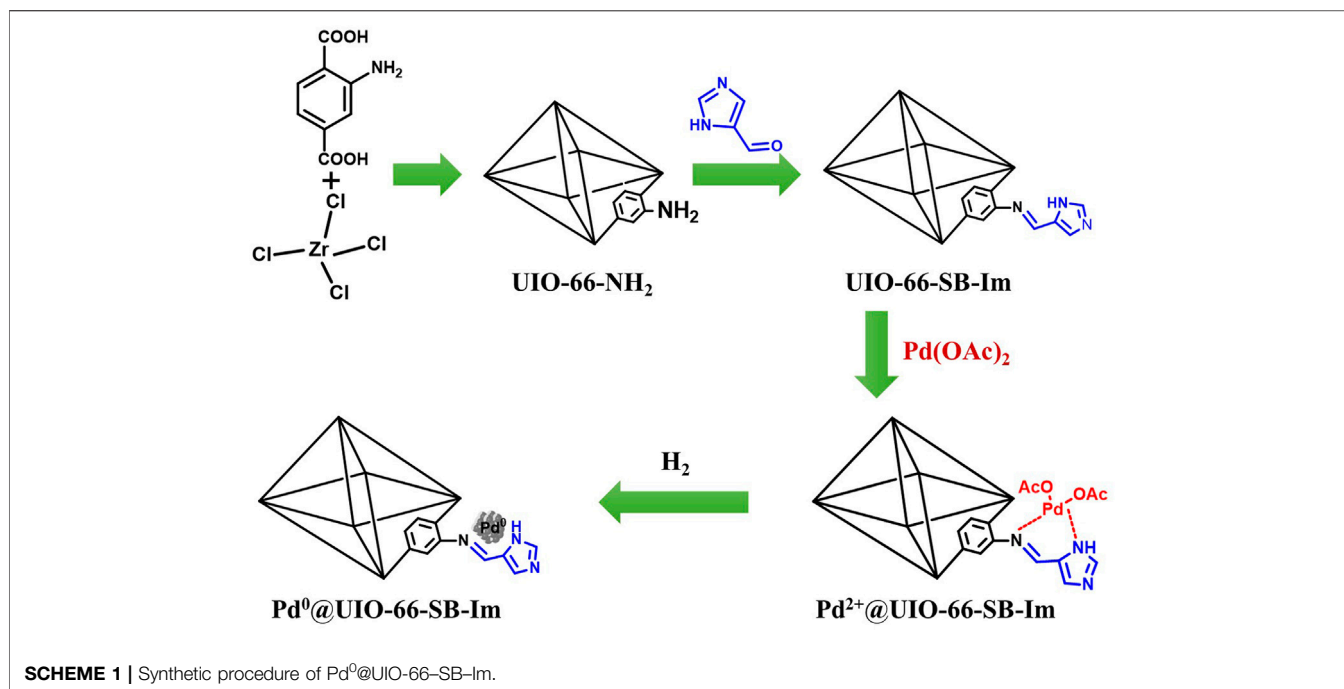
The preparation of UIO-66-SB-Im and immobilization of Pd⁰ species to UIO-66-SB-Im are illustrated in **Scheme 1**. Briefly, UIO-66-NH₂ was hydrothermally synthesized through the coordination of metal source (ZrCl₄) and organic linker (2-aminoterephthalic acid, H₂BDC-NH₂), followed by an aldimine condensation process with 4-imidazolecarboxaldehyde (Im-CHO) to yield UIO-66-SB-Im support. Pd⁰@UIO-66-SB-Im catalyst was prepared by incorporating the precursor Pd(OAc)₂ into the Schiff base-imidazole-functionalized MOFs *via* coordination and subsequent H₂ reduction. Elemental analyses indicate that the

N contents of UIO-66-NH₂ and UIO-66-SB-Im are 4.76% and 10.23%, respectively, implying the integration of Im-CHO moieties into the UIO-66-NH₂ matrix (**Table 1**). Pd²⁺@UIO-66-SB-Im and Pd⁰@UIO-66-SB-Im have a similar N content on the MOF skeleton, suggesting the stability of the surface groups and framework of UIO-66-SB-Im during the Pd immobilization process (**Table 1**). ICP analysis shows that Pd⁰@UIO-66-SB-Im contains a high Pd content of 2.3 wt%.

Power X-ray diffraction (PXRD) was used to characterize the crystallinity of the prepared samples. As shown in **Figure 1**, the experimental PXRD pattern of the synthesized UiO-66-NH₂ matches well with the simulated one (Gang et al., 2018), indicating the successful preparation of UiO-66-NH₂. After the aldimine condensation, the resulting product UIO-66-SB-Im performs the same PXRD pattern with UiO-66-NH₂, suggesting that the crystallinity and structure of MIL-101 are well retained after the postsynthesis. The crystallinity and structure are still retained after loading Pd(OAc)₂ and subsequent H₂ reduction. Moreover, the diffraction peak of Pd nanoparticles (NPs) at $2\theta = 40.1^\circ$ was not detected in Pd⁰@UIO-66-SB-Im, revealing that Pd NPs could be small.

Scanning electron microscopy (SEM) imaging shows that UIO-66-SB-Im (**Figure 2A**) performs similar morphology with UIO-66-NH₂, which is composed of nanometer-leveled particles with the size in range of 100–150 nm. After loading Pd species, the morphology of Pd²⁺@UIO-66-SB-Im and Pd⁰@UIO-66-SB-Im were retained (**Figures 2B, C**), implying that UIO-66-NH₂ is stable after functionalization. Elemental (Zr, N, and Pd) mapping images of Pd²⁺@UIO-66-SB-Im further prove the successful introduction of Pd species (**Figure 2D**). The TEM images and Pd size distribution of Pd⁰@UIO-66-SB-Im are given in **Figure 3E**. From the picture, the Pd clusters were uniformly distributed with average size of 1.5 nm, belonging to sub-2-nanometer size. Apart from this, the lattice spacing of Pd clusters was about 0.22 nm, ascribed to the Pd(111) crystal face (Zhao et al., 2014), which is active for Suzuki coupling reactions.

Quantitative porous properties of UIO-66-NH₂, UIO-66-SB-Im, Pd²⁺@UIO-66-SB-Im, and Pd⁰@UIO-66-SB-Im are established by the N₂ sorption analysis. **Figure 3** illustrates the N₂ sorption isotherms (**Figure 3A**) and corresponding pore size distribution curves (**Figure 3B**). The UIO-66-SB-Im exhibits similar N₂ sorption isotherms with UIO-66-NH₂ than a typical I type isotherm with a dramatic increase in nitrogen uptake in the partial pressure range of $p/p_0 < 0.1$, characteristic of classical microporosity (Chen et al., 2018). The BET (Brunauer–Emmett–Teller) surface area and the total pore volume of UIO-66-SB-Im are 537 m² g⁻¹ and 0.3 cm³ g⁻¹, respectively (**Table 1**). The decrease in the surface area and pore volume of UIO-66-SB-Im, in comparison with those of UIO-66-NH₂ (709 m² g⁻¹ with a volume of 0.40 cm³ g⁻¹), may be ascribed to the partial occupation of the cavities in NH₂-UIO-66 by the Schiff base and imidazole groups. The pore-size distribution curve calculated by the DFT (discrete Fourier transform) method further reveals the existence of micropores with a narrow pore size distribution in UIO-66-SB-Im. After

**TABLE 1** | Textural properties.

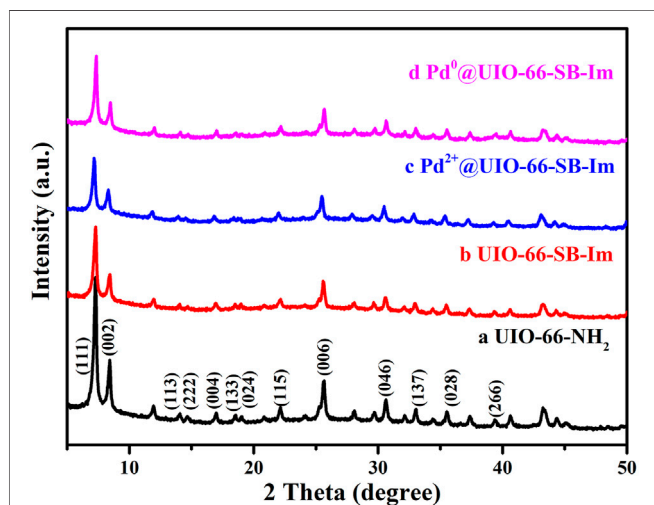
Samples	N% ^a	S _{BET} (m ² /g) ^b	V _p (cm ³ /g) ^c	D _p (nm) ^d
UIO-66-NH ₂	4.76	709	0.40	2.27
UIO-66-SB-Im	10.23	537	0.30	2.24
Pd ²⁺ @UIO-66-SB-Im	9.58	428	0.25	2.23
Pd ⁰ @UIO-66-SB-Im	9.74	452	0.26	2.23

Note. ^aThe content of N element.

^bBET surface area.

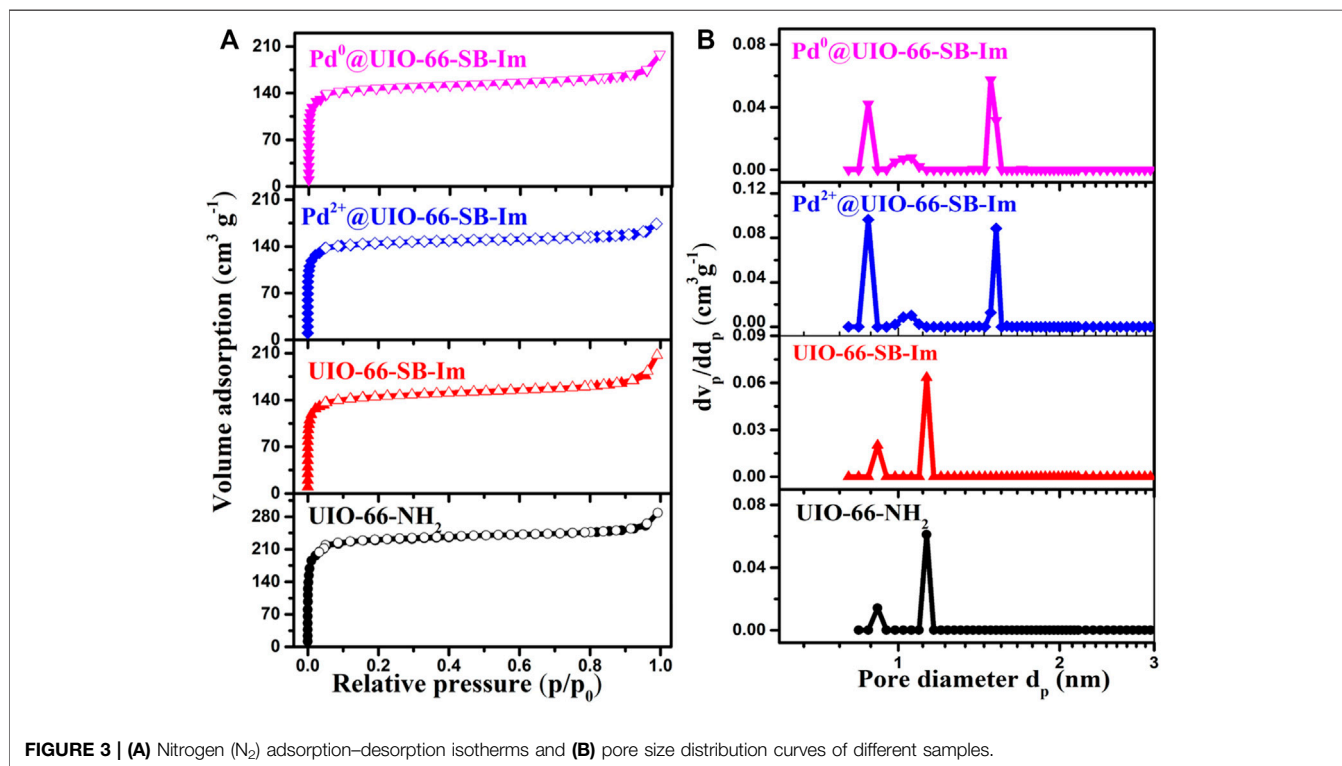
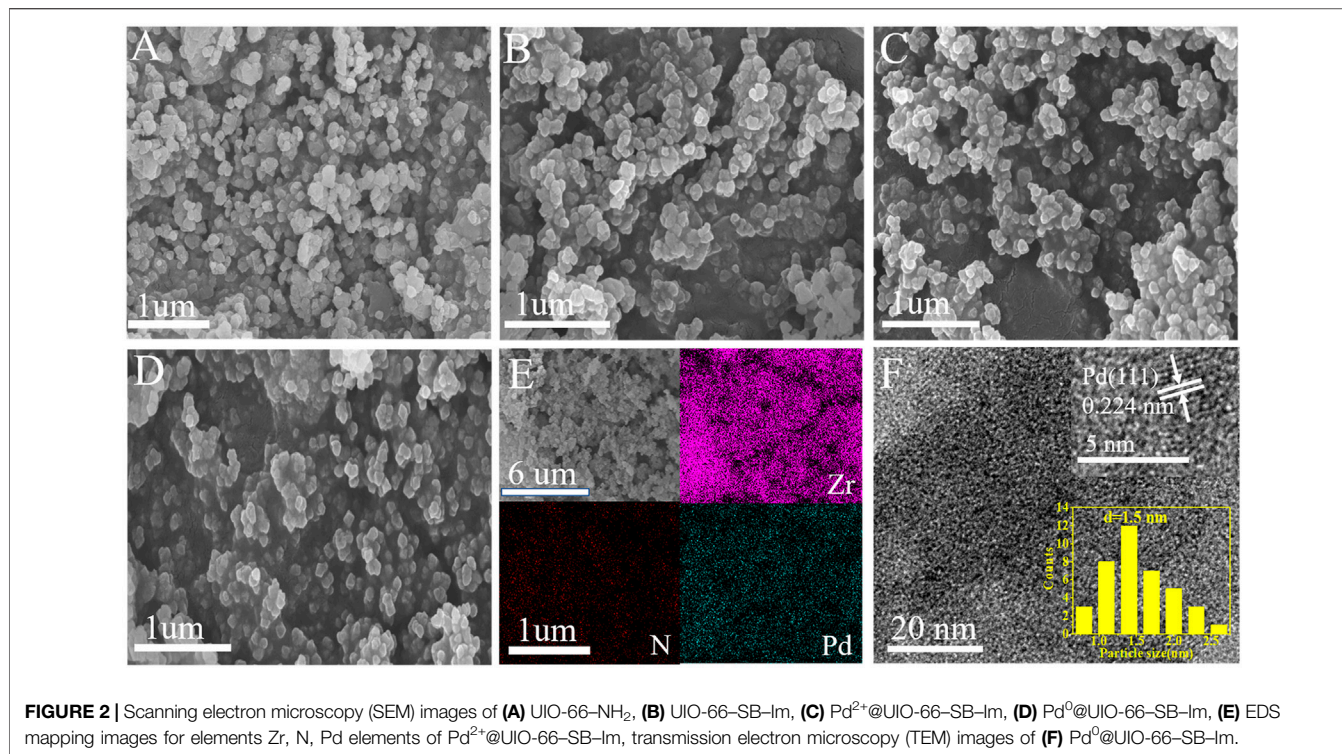
^cTotal pore volume.

^dAverage pore size.

**FIGURE 1** | Power X-ray diffraction (PXRD) diffraction patterns of UIO-66-NH₂, UIO-66-SB-Im, Pd²⁺@UIO-66-SB-Im, and Pd⁰@UIO-66-SB-Im.

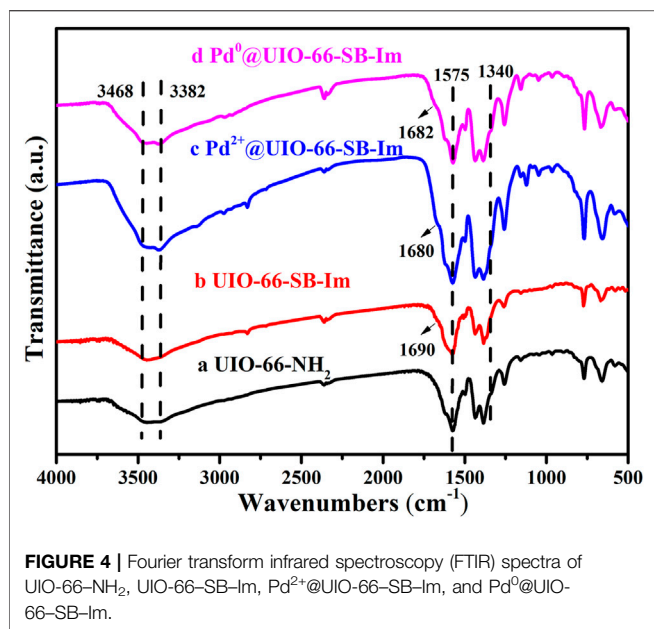
loading Pd, Pd²⁺@UIO-66-SB-Im and Pd⁰@UIO-66-SB-Im performs similar sorption isotherms with their parent UIO-66-SB-Im, revealing the preservation of porosity during the Pd-loading step. The BET surface areas of Pd²⁺@UIO-66-SB-Im and Pd⁰@UIO-66-SB-Im is 428 and 452 m²g⁻¹, respectively, which are smaller than that of UIO-66-SB-Im due to the partial pore filling by the deposited Pd species and the weakly decreased proportion of porous structure after Pd loading (Wang et al., 2016; Liu et al., 2021). The BET surface area and pore volume of Pd⁰@UIO-66-SB-Im increased slightly with subsequent H₂ reduction, which could be ascribed to the removal of OAc⁻ from the precursor during the reduction process (Liu et al., 2021).

The structure of the samples and the relationship between Pd and the support UIO-66-SB-Im were further analyzed by Fourier transform infrared spectroscopy (FTIR). As displayed in **Figure 4**, the FTIR spectrum of UIO-66-NH₂ shows a peak at 1,340 cm⁻¹ that attributed to the C-N stretch vibration on benzene ring (Lin et al., 2012), while those at 3,478 and 3,371 cm⁻¹ could be assigned to the asymmetric and symmetric vibrations of -NH₂, which further demonstrate the successful synthesis of UIO-66-NH₂ (Lin et al., 2012). After the aldimine condensation with Im-CHO, several peaks appeared in the FTIR spectrum of UIO-66-SB-Im compared with that of UIO-66-NH₂. The new peak at 1,648 cm⁻¹ could be ascribed to the stretch vibration of C=N and featured band of imidazole (Lin et al., 2012; Gang et al., 2018), indicating the successful introduction of Im-CHO and successful formation of Schiff base. After anchoring Pd(OAc)₂ on UIO-66-SB-Im, the peak at 1,648 cm⁻¹ corresponding to the Schiff base and imidazole groups is shifted to 1,675 cm⁻¹, suggesting the interaction of the Schiff base and imidazole groups in UIO-66-SB-Im with Pd(OAc)₂ (Wang et al., 2015; Liu et al., 2017). A similar

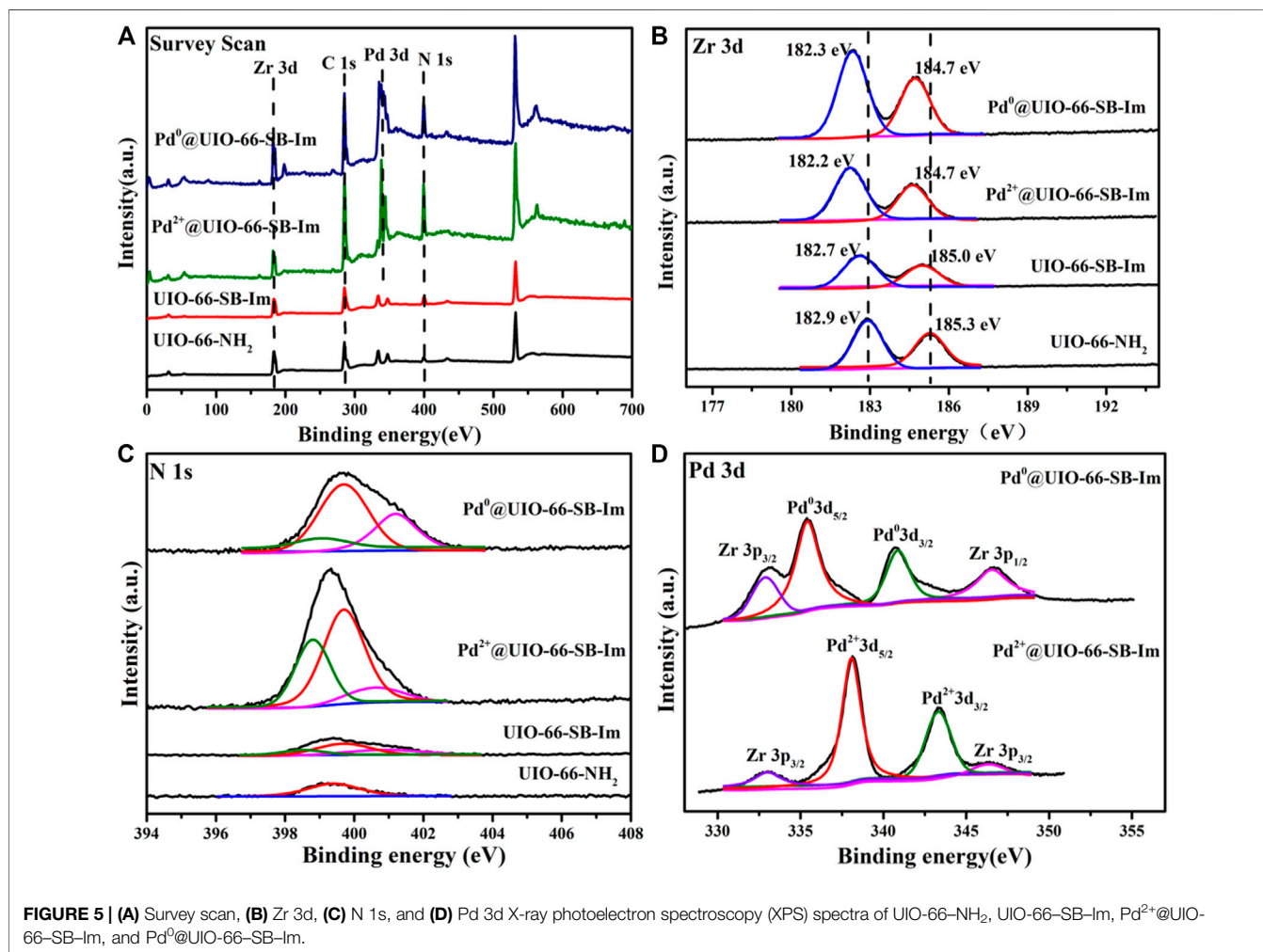


phenomenon occurred after H₂ reduction, implying the interaction of Schiff base and imidazole groups in UIO-66-SB-Im with Pd clusters.

Surface analyses of UIO-66-NH₂, UIO-66-SB-Im, Pd²⁺@UIO-66-SB-Im, and Pd⁰@UIO-66-SB-Im were carried out using X-ray photoelectron spectroscopy (XPS), and the results



are displayed in **Figure 5**. Three signals were observed at the binding energies of 181.5 eV (Zr3d), 228.4 eV (C1s), and 399.1 eV (N1s) in the survey scan XPS spectrum of UIO-66-SB-Im, manifesting the existence of Zr, C, and N elements (**Figure 5A**) (Gang et al., 2018). The high-resolution Zr3d XPS spectrum was deconvoluted into four peaks at 182.9 and 185.3 eV, which are ascribed to Zr3d_{5/2} and Zr3d_{3/2}, respectively (**Figure 5B**) (Gang et al., 2018). The high-resolution N1s XPS spectrum was fitted with three peaks at 398.2, 399.5, 400.6 eV, which correspond to the imine groups (-N=CH-) and imidazole N (Wang et al., 2015; Gang et al., 2018), respectively. After loading Pd, a new signal at binding energy of 338.7 eV (Pd3d) appeared in the survey scan XPS spectra of Pd²⁺@UIO-66-SB-Im and Pd⁰@UIO-66-SB-Im, further proving the successful introduction of Pd species into the support (**Figure 5A**). The high-resolution Zr3d XPS spectra of Pd²⁺@UIO-66-SB-Im and Pd⁰@UIO-66-SB-Im fitted likewise the two peaks with no other oxidation state of Zr peaks, indicating that the Zr was chemically stable during the functionalization of the linker and anchoring of Pd precursor (Gang et al., 2018). Moreover, compared with UIO-66-SB-Im,



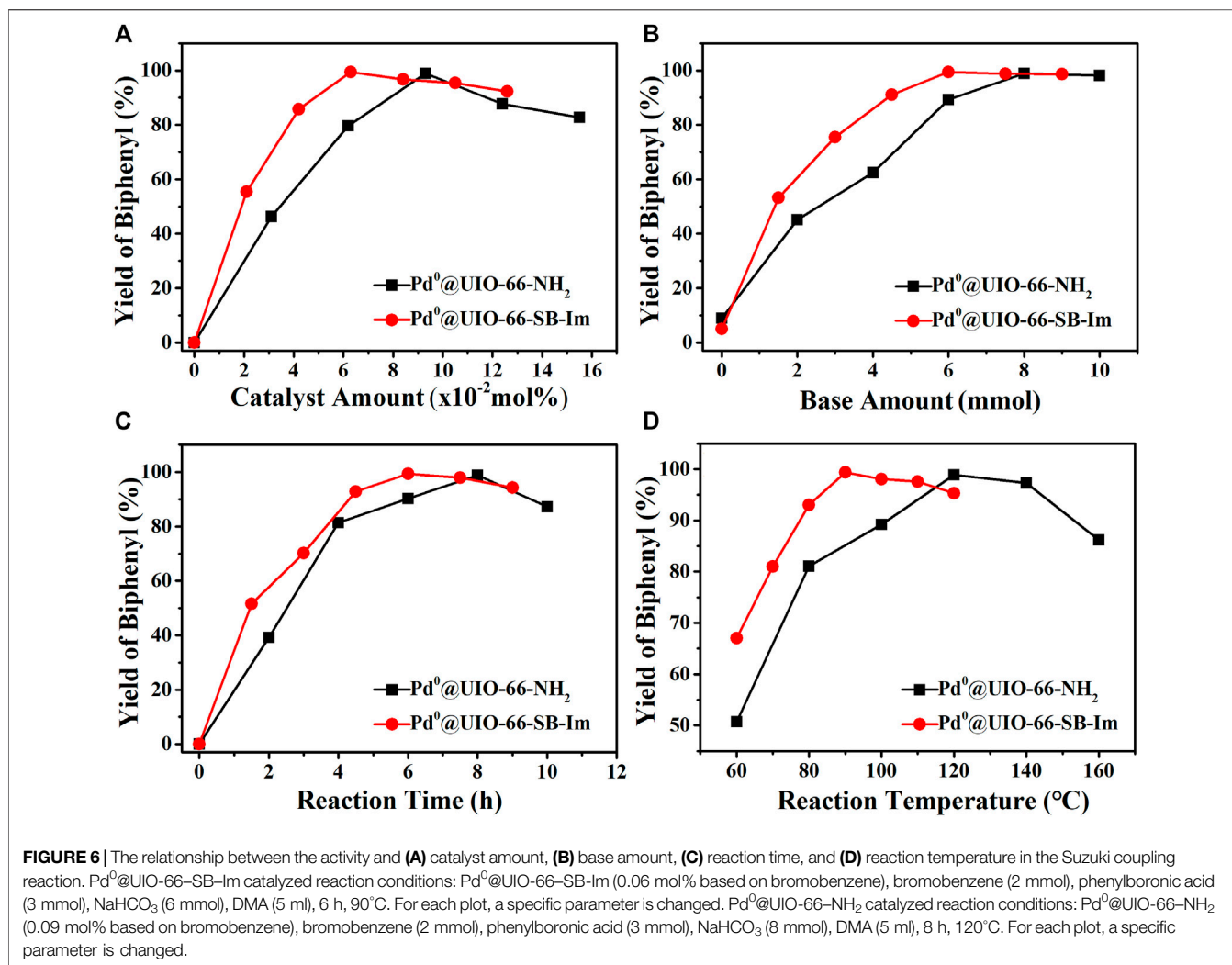


FIGURE 6 | The relationship between the activity and **(A)** catalyst amount, **(B)** base amount, **(C)** reaction time, and **(D)** reaction temperature in the Suzuki coupling reaction. Pd⁰@UIO-66-SB-Im catalyzed reaction conditions: Pd⁰@UIO-66-SB-Im (0.06 mol% based on bromobenzene), bromobenzene (2 mmol), phenylboronic acid (3 mmol), NaHCO₃ (6 mmol), DMA (5 ml), 6 h, 90°C. For each plot, a specific parameter is changed. Pd⁰@UIO-66-NH₂ catalyzed reaction conditions: Pd⁰@UIO-66-NH₂ (0.09 mol% based on bromobenzene), bromobenzene (2 mmol), phenylboronic acid (3 mmol), NaHCO₃ (8 mmol), DMA (5 ml), 8 h, 120°C. For each plot, a specific parameter is changed.

TABLE 2 | Catalytic performances of different catalysts for the Suzuki coupling reaction.

Entry ^a	Catalyst	Yield (%)
1	None	0
2	UIO-66-NH ₂	0
3	UIO-66-SB-Im	0
4	Pd ⁰ @UIO-66-SB-Im	95.3
5	Pd ⁰ @UIO-66-NH ₂	89.4

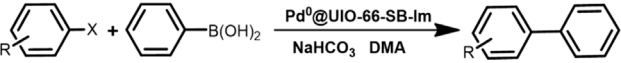
Note. ^aReaction conditions: catalyst (0.103 mol% based on bromobenzene), bromobenzene (2 mmol), phenylboronic acid (3 mmol), NaHCO₃ (4 mmol), DMA (5 ml), 7 h, 90°C.

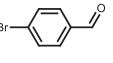
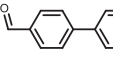
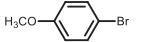
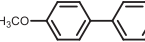
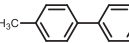
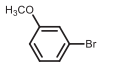
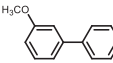
the peaks of Zr in Pd²⁺@UIO-66-SB-Im and Pd⁰@UIO-66-SB-Im was slightly shifted to lower energy. The phenomenon implies that the oxidation state of Zr⁴⁺ in Pd²⁺@UIO-66-SB-Im and Pd⁰@UIO-66-SB-Im was reduced, which may be due to the electron transfer from Pd to Zr on the support (Gang et al., 2018). The high-resolution NIs XPS spectra of Pd²⁺@UIO-66-SB-Im was fitted with three peaks at 398.5, 399.8, and 400.9 eV, which shift positively by 0.3 eV compared with

UIO-66-SB-Im. The phenomenon indicates the interaction of Schiff base and imidazole with Pd (Liu et al., 2017). The high-resolution Pd3d XPS spectrum of Pd²⁺@UIO-66-SB-Im exhibits two peaks at 338.1 and 343.5 eV, assignable to Pd²⁺3d_{5/2} and Pd²⁺3d_{3/2}, respectively, indicating that the surface Pd species of Pd²⁺@UIO-66-SB-Im are in a Pd²⁺ state (Figure 5D) (Liu et al., 2017; Liu et al., 2018). After reduction, Pd⁰@UIO-66-SB-Im exhibits only two Pd⁰3d peaks at 335.5 (3d_{5/2}) and 340.8 eV (3d_{3/2}), implying that Pd species of Pd⁰@UIO-66-SB-Im are all in the metallic state (Figure 5D) (Liu et al., 2021).

Enhanced Catalytic Activity in the Suzuki Coupling Reaction

The catalytic performance of Pd⁰@UIO-66-SB-Im was assessed in the Suzuki coupling reaction between bromobenzene and phenylboronic acid at mild conditions. The activities of different catalysts were parallel investigated under the same reaction conditions, and the results are summarized in Table 2. The reaction does not proceed in the absence of catalysts or catalyzed by the pure support UIO-66-NH₂ or

TABLE 3 | Suzuki coupling reactions of various aryl halide with phenylboronic acid using Pd⁰@UIO-66-SB-Im as the catalyst.


Entry ^a	Substrate	Product	Yield (%) ^b
1			>99
2			>99
3			>99
4			87.9
5			85.4
6			86.3
7			>99
8			37

Note. ^aReaction condition: Pd⁰@UIO-66-SB-Im (0.06 mol% based on bromobenzene), aryl halides (2 mmol), phenylboronic acid (3 mmol), NaHCO₃ (6 mmol), DMA (5 ml), 6 h, 90°C.

^bThe yield of biphenyl was determined by gas chromatograph (GC) with 1,4-dioxane used as an internal standard.

UIO-66-SB-Im (Table 2, entries 1–3). The material Pd⁰@UIO-66-SB-Im behaved with 95.3% yield of biphenyl, indicating that the Pd⁰ species are the active species in the reaction (Table 2, entry 4). Moreover, the contrast catalyst Pd⁰@UIO-66-NH₂ was synthesized and investigated in the reaction. Pd⁰@UIO-66-NH₂ only performed 89.4% yield of biphenyl (Table 2, entry 5). The results show that the Pd⁰@UIO-66-NH₂ is the best catalyst for the reaction.

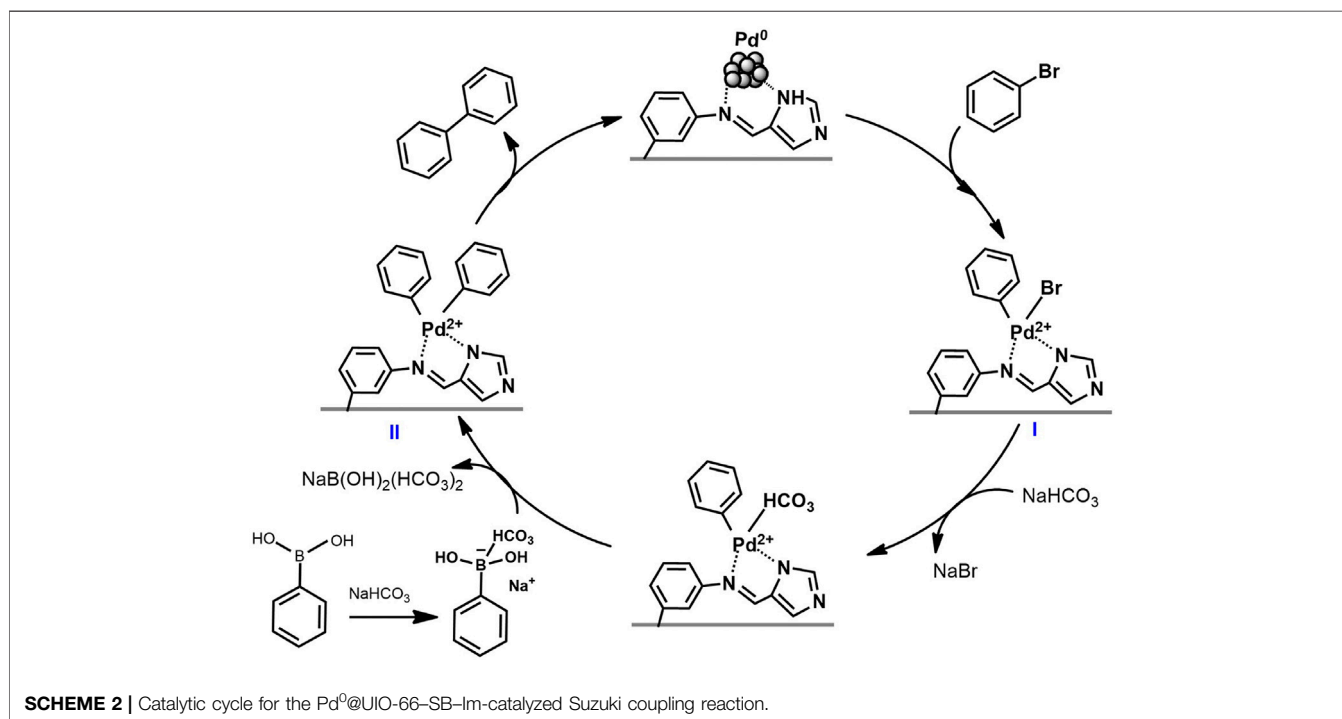
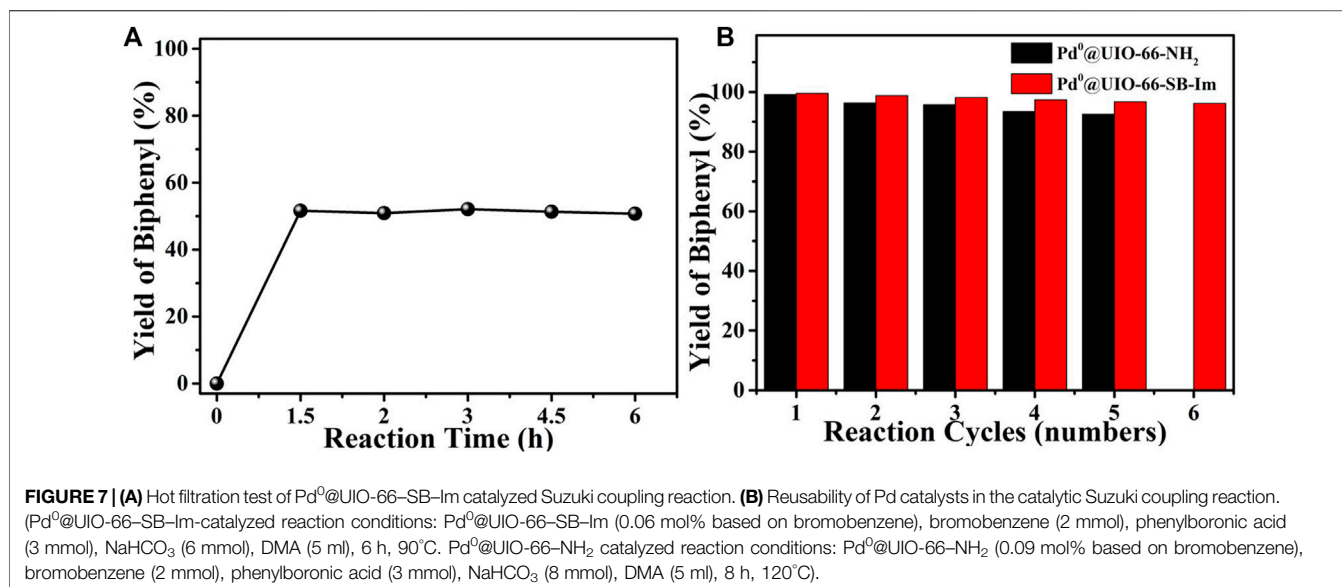
The Suzuki coupling of bromobenzene and phenylboronic acid to biphenyl was further investigated by using the catalyst Pd⁰@UIO-66-SB-Im under different reactions with respect to the amount of catalyst, the amount of base, the reaction time, and the reaction temperature (Figure 6). Moreover, Pd⁰@UIO-66-NH₂ was also parallel investigated for comparison (Figure 6). The yield as the function of the catalyst amount exhibits a “volcanic” type curve. Initially, the yield initially increases gradually when the catalyst amount increases (Figure 6A). At up to 0.063 mol%, the yield reaches the highest value of 99.4%. A further increase in the catalyst amount causes a slight decrease in yield that could be attributed to the over-oxidation of the product along with the reaction (Lin et al., 2012). For Pd⁰@UIO-66-NH₂, more catalyst dosage (0.093 mol%) was needed to reach the highest biphenyl yield, and the yield is only 98.9%. Fixing the catalyst amount of Pd⁰@UIO-66-SB-Im at 0.063 mol%, the base NaHCO₃ amount

was studied (Figure 6B). A higher number of base favors higher biphenyl yield. In view of environmental impact, 6 mmol is suitable. For Pd⁰@UIO-66-NH₂, more amount of base is needed (>8 mmol) to reach the yield of 99%, which will cause more waste of chemicals and is environmentally unfriendly (Figure 6B). The survey of the reaction time and temperature suggests that moderate reaction time (6 h) and temperature (90°C) benefit high yield of biphenyl because of the over-oxidation with elongating time or higher temperature (Figures 5E, F). The above investigation shows that Pd⁰@UIO-66-SB-Im is highly efficient for the Suzuki coupling reaction under mild condition. Compared with Pd⁰@UIO-66-NH₂, the superior activity of Pd⁰@UIO-66-NH₂-MC is probably ascribed to the cooperation between Pd⁰ clusters and the Schiff base-imidazole-functionalized UIO-66-SB-Im.

The scope of Pd⁰@UIO-66-SB-Im is further extended to the Suzuki coupling of various aryl halides with phenylboronic acid (Table 3). Pd⁰@UIO-66-SB-Im-catalyzed coupling of bromobenzene with electron-withdrawing groups (nitro, aldehyde, or methoxy group) performed high yields of the corresponding biphenyl products (Table 3, entries 1–3), while coupling of bromobenzene bearing electron-donating groups (methyl group) behaved with lower yields to the coupling products (Table 3, entries 4–6), implying that the withdrawing groups in bromobenzene is beneficial to the reaction, while the electron-donating groups in bromobenzene is harmful (Shang et al., 2014). Coupling of aryl iodobenzene with phenylboronic acid produced >99% yield of biphenyl (Table 3, entry 7), while coupling of chlorobenzene only obtained 37% yield of biphenyl (Table 3, entry 8) because the C–X (X = Cl, Br, I) bond dissociation energy is C–Cl > C–Br > C–I (Lin et al., 2012; Shang et al., 2014).

In order to investigate the heterogeneous nature of Pd⁰@UIO-66-SB-Im, a hot filtration test was carried out and is shown in Figure 7A. A reaction catalyzed by Pd⁰@UIO-66-SB-Im was prematurely stopped at 1.5 h (i.e., 51.6% biphenyl yield by GC analysis), and then the solid catalyst was removed by hot filtration. The filtrate was engaged in the additional reaction for an additional 4.5 h, and no more biphenyl was produced as analyzed by GC, confirming that the reaction proceeds on the solid surface of the catalyst and excludes the contribution of the possible leached Pd species. By simple filtration, the catalyst can be facilely separated and reused in the next time. As shown in Figure 7B, the catalyst Pd⁰@UIO-66-SB-Im could be reused for six times without significant decrease in performance, while the recycled catalyst Pd⁰@UIO-66-NH₂ performed obvious decrease, further implying the well stability of Pd⁰ species anchored on the Schiff base-imidazole-functionalized UIO-66-SB-Im. As demonstrated by the XRD and FTIR spectra of the spent catalyst Pd⁰@UIO-66-SB-Im after six runs, the crystalline structure and the polymeric network were preserved (Supplementary Figures S1 and S2). TEM images show that the Pd⁰ clusters of Pd⁰@UIO-66-SB-Im^{6th} have grown, which may lead to the slight decrease in catalytic performance (Supplementary Figure S3).

A reaction route of the Suzuki coupling catalyzed by Pd⁰@UIO-66-SB-Im is proposed by combining the catalytic results



and previous mechanism studies (Lin et al., 2012; Shang et al., 2014). As shown in **Scheme 2**, in the first step, Pd⁰ clusters stabilized by the Schiff base and imidazole groups on the surface of UIO-66-SB-Im interact with the electrophilic reagent bromobenzene to form organo-palladium species (I) by oxidative addition. Then the organo-palladium species (I) reacts with the other reactant phenylboronic acid through transmetalation in the presence of a base to produce an intermediate (II). Finally, biphenyl is produced, and Pd(II) is

reduced to the original Pd⁰ state through the reductive elimination of (II).

CONCLUSION

Highly dispersed Pd⁰ clusters anchored on MOFs was successfully synthesized by postsynthetic modification. The surface groups of Schiff base and imidazole groups that

grafted on the MOFs are found to play a vital role in the control of small Pd clusters with an average size of only 1.5 nm. The catalyst Pd⁰@UO-66-SB-Im exhibited excellent performance in the Suzuki coupling reaction of halogenated benzene with phenylboronic acid. Moreover, the catalyst behaved well with substrate compatibility and good reusability.

DATA AVAILABILITY STATEMENT

All datasets generated for this study are included in the article/**Supplementary Material**.

AUTHOR CONTRIBUTIONS

YL and JS contributed to the nanomaterials' entire design and synthesis. LF and QX guided the idea, analyzed the data, and drafted the manuscript. All authors read and improved the manuscript. All authors read and approved the final manuscript.

REFERENCES

- Chen, M. J., Chang, G. G., Chen, L. Y., Huang, K. X., Pu, C., Li, D., et al. (2021). Multifunctional Pd/MOFs@MOFs Confined Core-Shell Catalysts with Wrinkled Surface for Selective Catalysis. *Chem. Asian J.* 16, 3743–3747. doi:10.1002/asia.202100922
- Chen, X., Shen, K., Ding, D., Chen, J. Y., Chen, J., Wu, R. F., et al. (2018). Solvent-Driven Selectivity Control to Either Anilines or Dicyclohexylamines in Hydrogenation of Nitroarenes over a Bifunctional Pd/MIL-101 Catalyst. *ACS Catal.* 8, 10641–10648. doi:10.1021/acscatal.8b01834
- Diez, I., and Ras, R. H. A. (2011). Fluorescent Silver Nanoclusters. *Nanoscale* 3, 1963–1970. doi:10.1039/C1NR00006C
- Dong, Y., Ying, J., Xiao, Y. X., Chen, J. B., and Yang, X. Y. (2021). Highly Dispersed Pt Nanoparticles Embedded in N-Doped Porous Carbon for Efficient Hydrogen Evolution. *Chem. Asian J.* 16, 1878–1881. doi:10.1002/asia.202100438
- Eid, K., Sliem, M. H., Eldesoky, A. S., Al-Kandari, H., and Abdullah, A. M. (2019). Rational Synthesis of One-Dimensional Carbon Nitride-Based Nanofibers Atomically Doped with Au/Pd for Efficient Carbon Monoxide Oxidation. *Int. J. Hydrogen Energ.* 44, 17943–17953. doi:10.1016/j.ijhydene.2019.05.105
- Fang, X. Z., Shang, Q. C., Wang, Y., Jiao, L., Yao, T., Li, Y. F., et al. (2018). Single Pt Atoms Confined Into a Metal-Organic Framework for Efficient Photocatalysis. *Adv. Mater.* 30, 1705112. doi:10.1002/adma.201705112
- Furukawa, H., Cordova, K. E., O'Keeffe, M., and Yaghi, O. M. (2013). The Chemistry and Applications of Metal-Organic Frameworks. *Science* 341, 6149. doi:10.1126/science.1230444
- Gu, Y., Chen, X., Cao, Y., Zhuang, G., Zhong, X., and Wang, J. (2017). Atomically Dispersed Pd Catalysts in Graphyne Nanopore: Formation and Reactivity. *Nanotechnology* 28, 295403. doi:10.1088/1361-6528/aa7764
- Guo, Z., You, Q., Song, L., Sun, G., Chen, G., Li, C., et al. (2021). Highly Dispersed Pt Species Anchored onto NH₂-Ce-MOFs and Their Derived Mesoporous Catalysts for CO Oxidation. *Nanoscale* 13, 117–123. doi:10.1039/D0NR05626J
- Han, Y., Xu, H., Su, Y., Xu, Z.-L., Wang, K., and Wang, W. (2019). Noble Metal (Pt, Au@Pd) Nanoparticles Supported on Metal Organic Framework (MOF-74) Nanoshuttles as High-Selectivity CO₂ Conversion Catalysts. *J. Catal.* 370, 70–78. doi:10.1016/j.jcat.2018.12.005
- He, T., Chen, S., Ni, B., Gong, Y., Wu, Z., Song, L., et al. (2018). Zirconium-porphyrin-based Metal-Organic Framework Hollow Nanotubes for Immobilization of Noble-metal Single Atoms. *Angew. Chem. Int. Ed.* 57, 3493–3498. doi:10.1002/anie.201800817
- Imaoka, T., Akanuma, Y., Haruta, N., Tsuchiya, S., Ishihara, K., Okayasu, T., et al. (2017). Platinum Clusters with Precise Numbers of Atoms for Preparative-Scale Catalysis. *Nat. Commun.* 8, 688. doi:10.1038/s41467-017-00800-4

FUNDING

The authors thank the National Natural Science Foundation of China (21802119), National Key Research and Development Program (2016YFC0209203), the Joint Open Fund of Jiangsu Collaborative Innovation Center for Ecological Building Material and Environmental Protection Equipment, and Key Laboratory for Advanced Technology in Environmental Protection of Jiangsu Province (JH201806), and Funding for school-level research projects of Yancheng Institute of Technology (xjr2019005).

SUPPLEMENTARY MATERIAL

The Supplementary Material for this article can be found online at: <https://www.frontiersin.org/articles/10.3389/fchem.2022.845274/full#supplementary-material>

- Khan, F. U., Mehmood, S., Liu, S., Xu, W., Shah, M. N., Zhao, X., et al. (2021). A P-N Heterojunction Based Pd/PdO@ZnO Organic Frameworks for High-Sensitivity Room-Temperature Formaldehyde Gas Sensor. *Front. Chem.* 9, 742488. doi:10.3389/fchem.2021.742488
- Lee, J., Farha, O. K., Roberts, J., Scheidt, K. A., Nguyen, S. T., and Hupp, J. T. (2009). Metal-organic Framework Materials as Catalysts. *Chem. Soc. Rev.* 38, 1450–1459. doi:10.1039/B807080F
- Li, J.-R., Sculley, J., and Zhou, H.-C. (2012). Metal-organic Frameworks for Separations. *Chem. Rev.* 112, 869–932. doi:10.1021/cr200190s
- Lin, Y., Kong, C., and Chen, L. (2012). Direct Synthesis of Amine-Functionalized MIL-101(Cr) Nanoparticles and Application for CO₂ Capture. *RSC Adv.* 2, 6417–6419. doi:10.1039/c2ra20641b
- Liu, J., Ma, Q., Huang, Z., Liu, G., and Zhang, H. (2019). Recent Progress in Graphene-Based noble-metal Nanocomposites for Electrocatalytic Applications. *Adv. Mater.* 31, 1800696. doi:10.1002/adma.201800696
- Liu, Y., Wang, K., Hou, W., Shan, W., Li, J., Zhou, Y., et al. (2018). Mesoporous Poly(ionic Liquid) Supported Palladium(II) Catalyst for Oxidative Coupling of Benzene Under Atmospheric Oxygen. *Appl. Surf. Sci.* 427, 575–583. doi:10.1016/j.apsusc.2017.08.019
- Liu, Y., Zhou, Y., Li, J., Wang, Q., Qin, Q., Zhang, W., et al. (2017). Direct Aerobic Oxidative Homocoupling of Benzene to Biphenyl Over Functional Porous Organic Polymer Supported Atomically Dispersed Palladium Catalyst. *Appl. Catal. B: Environ.* 209, 679–688. doi:10.1016/j.apcatb.2017.03.029
- Liu, Y., Zou, C., Wang, K., Bian, Z., Jiang, S., Zhou, Y., et al. (2021). Palladium Clusters on Dicarboxyl-Functional Hypercrosslinked Porous Polymers for Oxidative Homocoupling of Benzene with O₂. *Mol. Catal.* 505, 111487. doi:10.1016/j.mcat.2021.111487
- Mouarrawis, V., Plessius, R., van der Vlugt, J. I., and Reek, J. N. H. (2018). Confinement Effects in Catalysis Using Well-Defined Materials and Cages. *Front. Chem.* 6, 623. doi:10.3389/fchem.2018.00623
- Peng, H., Dong, T., Zhang, L., Wang, C., Liu, W., Bao, J., et al. (2019). Active and Stable Pt-Ceria Nanowires@silica Shell Catalyst: Design, Formation Mechanism and Total Oxidation of CO and Toluene. *Appl. Catal. B: Environ.* 256, 117807. doi:10.1016/j.apcatb.2019.117807
- Shang, N., Gao, S., Zhou, X., Feng, C., Wang, Z., and Wang, C. (2014). Palladium Nanoparticles Encapsulated inside the Pores of a Metal-Organic Framework as a Highly Active Catalyst for Carbon-Carbon Cross-Coupling. *RSC Adv.* 4, 54487–54493. doi:10.1039/c4ra10065d
- Si, J., Xiao, S., Wang, Y., Zhu, L., Xia, X., Huang, Z., et al. (2018). Sub-nanometer Co₃O₄ Clusters Anchored on TiO₂(B) Nano-Sheets: Pt Replaceable Co-catalysts for H₂ Evolution. *Nanoscale* 10, 2596–2602. doi:10.1039/C7NR07336D
- Su, J., Yuan, S., Wang, T., Lollar, C. T., Zuo, J.-L., Zhang, J., et al. (2020). Zirconium Metal-Organic Frameworks Incorporating Tetrathiafulvalene Linkers: Robust

- and Redox-Active Matrices for In Situ Confinement of Metal Nanoparticles. *Chem. Sci.* 11, 1918–1925. doi:10.1039/C9SC06009J
- Tang, Q., Lee, Y., Li, D.-Y., Choi, W., Liu, C. W., Lee, D., et al. (2017). Lattice-Hydride Mechanism in Electrocatalytic CO₂ Reduction by Structurally Precise Copper-Hydride Nanoclusters. *J. Am. Chem. Soc.* 139, 9728–9736. doi:10.1021/jacs.7b05591
- Wang, J., Yang, M., Dong, W., Jin, Z., Tang, J., Fan, S., et al. (2016). Co(ii) Complexes Loaded into Metal-Organic Frameworks as Efficient Heterogeneous Catalysts for Aerobic Epoxidation of Olefins. *Catal. Sci. Technol.* 6, 161–168. doi:10.1039/c5cy01099c
- Wang, X., Li, J., Chen, G., Guo, Z., Zhou, Y., and Wang, J. (2015). Hydrophobic Mesoporous Poly(ionic Liquid)s towards Highly Efficient and Contamination-Resistant Solid-Base Catalysts. *ChemCatChem* 7, 993–1003. doi:10.1002/cctc.201402995
- Wang, Y., Su, Y.-Q., Hensen, E. J. M., and Vlachos, D. G. (2020). Finite-temperature Structures of Supported Subnanometer Catalysts Inferred via Statistical Learning and Genetic Algorithm-Based Optimization. *ACS Nano* 14, 13995–14007. doi:10.1021/acsnano.0c06472
- Xin, P., Li, J., Xiong, Y., Wu, X., Dong, J., Chen, W., et al. (2018). Revealing the Active Species for Aerobic Alcohol Oxidation by Using Uniform Supported Palladium Catalysts. *Angew. Chem. Int. Ed.* 57, 4642–4646. doi:10.1002/anie.201801103
- Xiong, G., Chen, X.-L., You, L.-X., Ren, B.-Y., Ding, F., Dragutan, I., et al. (2018). La-Metal-Organic Framework Incorporating Fe₃O₄ Nanoparticles, post-synthetically Modified with Schiff Base and Pd. A Highly Active, Magnetically Recoverable, Recyclable Catalyst for C C Cross-Couplings at Low Pd Loadings. *J. Catal.* 361, 116–125. doi:10.1016/j.jcat.2018.02.026
- Yamamoto, K., Imaoka, T., Tanabe, M., and Kambe, T. (2020). New Horizon of Nanoparticle and Cluster Catalysis with Dendrimers. *Chem. Rev.* 120 (2), 1397–1437. doi:10.1021/acs.chemrev.9b00188
- Yang, C., Zhao, Z., and Liu, Q. (2021). Mechanistic Insight into the Dispersion Behavior of Single Platinum Atom on Monolayer G-C₃N₄ in Single-Atom Catalysts from Density Functional Theory Calculations. *Appl. Surf. Sci.* 566, 150697. doi:10.1016/j.apsusc.2021.150697
- Zhang, F., Zheng, S., Xiao, Q., Zhong, Y., Zhu, W., Lin, A., et al. (2016). Synergetic Catalysis of Palladium Nanoparticles Encaged within Amine-Functionalized UiO-66 in the Hydrodeoxygenation of Vanillin in Water. *Green. Chem.* 18, 2900–2908. doi:10.1039/c5gc02615f
- Zhang, X., Zhang, X., Yang, P., and Jiang, S. P. (2021). Pt Clusters Embedded in G-C₃N₄ Nanosheets to Form Z-Scheme Heterostructures with Enhanced Photochemical Performance. *Surf. Inter.* 27, 101450. doi:10.1016/j.surfin.2021.101450
- Zhao, X., Jin, Y., Zhang, F., Zhong, Y., and Zhu, W. (2014). Catalytic Hydrogenation of 2,3,5-trimethylbenzoquinone over Pd Nanoparticles Confined in the Cages of MIL-101(Cr). *Chem. Eng. J.* 239, 33–41. doi:10.1016/j.cej.2013.11.003

Conflict of Interest: LF was employed by Yancheng Lanfeng Environmental Engineering Technology Co., Ltd.

The remaining authors declare that the research was conducted in the absence of any commercial or financial relationships that could be construed as a potential conflict of interest.

Publisher's Note: All claims expressed in this article are solely those of the authors and do not necessarily represent those of their affiliated organizations, or those of the publisher, the editors, and the reviewers. Any product that may be evaluated in this article, or claim that may be made by its manufacturer, is not guaranteed nor endorsed by the publisher.

Copyright © 2022 Liu, Sun, Fan and Xu. This is an open-access article distributed under the terms of the Creative Commons Attribution License (CC BY). The use, distribution or reproduction in other forums is permitted, provided the original author(s) and the copyright owner(s) are credited and that the original publication in this journal is cited, in accordance with accepted academic practice. No use, distribution or reproduction is permitted which does not comply with these terms.